Ventricular-Arterial Coupling and Mechanism of Wave Reflections

Julio A. Chirinos and Patrick Segers

Abstract

In this chapter, we discuss two approaches to quantitatively assess ventricular-arterial interaction: (i) the "classic" approach based on matching of ventricular and arterial elastance (analysis in pressure-volume plane) and (ii) a novel approach based on assessment of time-varying myocardial stress. The latter analysis, in the time domain, allows to directly link left ventricular myocardial stress with systemic arterial properties and with the magnitude and timing of arterial wave reflections.

Introduction

The interactions between the left ventricle (LV) and the systemic arteries are key determinants of cardiovascular function, dysfunction, and various cardiovascular disease states. This chapter deals with approaches used for the assessment of ventricular-arterial interactions and coupling,

J.A. Chirinos, MD, PhD
Philadelphia Veterans Affairs Medical Center, University of Pennsylvania School of Medicine, Philadelphia, PA, USA
e-mail: julio.chirinos@uphs.upenn.edu

P. Segers, PhD (✉)
Institute Biomedical Technology (IBiTech), iMinds Medical IT, Ghent University, Campus Heymans-Blok B, De Pintelaan 185, Ghent 9000, Belgium
e-mail: patrick.segers@ugent.be

with a focus on underlying hemodynamic principles and the interpretation of commonly used physiologic indices. We also review recent studies assessing the association between ventricular-arterial coupling, myocardial function, and heart failure risk in large populations.

Ventricular-Arterial Coupling: Matching Elastances?

Ventricular-arterial coupling is still most often associated with the study of ventricular (E_{es}) and arterial elastance (E_a) and of their ratio, introduced in the early 1980s [1]. E_{es}, end-systolic elastance, is the slope of the end-systolic pressure-volume relation [2], which is usually considered the gold standard measure of ventricular contractility and chamber function. It is
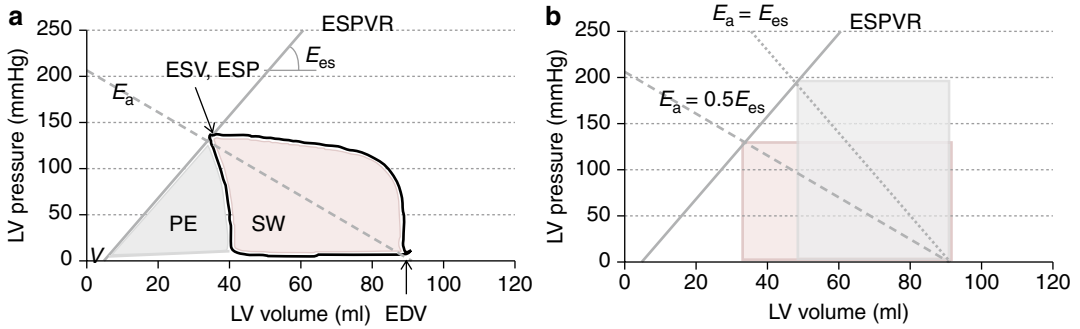
Fig. 4.1 Panel (**a**) Left ventricular pressure-volume (PV) loop with indication of the slope (E_{es}) and intercept (V_0) of the end-systolic pressure-volume relation (*ESPVR*) and the arterial elastance (E_a). The area enclosed by the PV loop represents the stroke work (*SW*), the *gray* area the

"potential" energy (*PE*). The sum of SW and PE is the pressure-volume area (PVA). Panel (**b**) Schematic of the PV loop associated with E_a/E_{es} of 1 (maximal SW generation) and E_a/E_{es} of 0.5 (maximal efficiency)

typically measured invasively using a pressure-volume (conductance) catheter, where the preload of the heart is progressively reduced via inflation of a balloon in the inferior vena cava. When considering the pressure-volume (PV) plane and assuming known end-systolic pressure-volume relation and end-diastolic volume (EDV) (and intact cardiac valves), the PV loop – and thus the operating conditions of the cardiovascular system – is fully determined with knowledge of the upper left-hand corner of the PV loop (end-systolic pressure, ESP, and end-systolic volume, ESV). The line connecting this point with the EDV point on the *y*-axis – thus having a slope [ESP/stroke volume] – can be approximated as *R/T*, with *R* the systemic vascular resistance and *T* the cardiac period. The slope, having mmHg/ml as units, has been termed the arterial elastance, E_a [1, 3]. Knowledge of E_a and E_{es} provides an elegant and intuitive (graphical or analytical) way to study the interaction between the heart and the arterial system in the PV plane (Fig. 4.1). The impact of changes in preload, afterload (*R*), cardiac frequency, and contractility on cardiac function (stroke volume and pressure development) is easily calculated and visualized. In addition, the PV plane provides a straightforward way to link ventricular function to mechanical performance [4]. The area enclosed by the PV loop (Fig. 4.1) is the stroke work (SW), while the area enclosed by the end-diastolic and end-systolic PV relation and descending limb of the PV loop is the

"potential energy (PE)," although the terminology "potential" is to be interpreted in a negative sense, as it represents the energy associated with pressurizing the non-ejected volume in the ventricular cavity, and therefore not used for perfusion. Animal studies demonstrated that the sum of the SW and PE (termed the pressure-volume area; PVA) is proportional to the myocardial oxygen consumption when the latter is manipulated by various interventions in single animals [5]. This global PV-based framework now provides a way to study the relation between the energetic output of the ventricle (SW) and the total energy provided to the heart (i.e., the efficiency of conversion of ATP into mechanical work) and this in terms of a "coupling parameter" E_a/E_{es}. This parameter is extensively used in studies considering mechanico-energetic aspects of heart-arterial coupling [4, 6, 7]. E_a/E_{es} varies over the range of 0.5 (optimal efficiency) to 1 (maximal stroke work generation) [4], while in heart failure with reduced ejection fraction, with dilated hearts, E_a/E_{es} becomes larger than one [7, 8]. This approach is highly attractive because of its simplicity, but there are some issues that deserve closer attention:

(i) The concept is based on experimental measurements in open-chest anesthetized animals, which might not be fully representative of normal human physiology. It has been demonstrated that the end-systolic pressure-volume relation is nonlinear rather than linear and sensitive to loading conditions [9].

(ii) The method is difficult to apply in practice. It is, at present, impossible to measure complete left ventricular pressure-volume loops in a noninvasive way. Part of the pressure-volume loop may, however, be obtained from aortic pressure and flow. Ultrasound technology may be used to estimate left ventricular end-systolic and/or end-diastolic dimensions or ejection fraction, though the accuracy is rather limited. In healthy subjects, there is little pressure drop over the aortic valve: aortic and left ventricular pressure can be assumed equal during ejection. Knowing left ventricular end-diastolic volume (EDV) and integrating aortic flow, part of the left ventricular pressure-volume loop can thus be obtained in a noninvasive way. Magnetic resonance imaging may provide a solution for noninvasive measurement of instantaneous ventricular volume. It is, however, difficult to obtain sufficiently large alterations of pre- or afterload without invasive interventions (such as the inflation of a balloon in the inferior vena cava to reduce cardiac filling and preload).

(iii) While the terminology of E_a as arterial elastance suggests that the parameter is related to arterial stiffness, it is not. In addition, E_a is highly determined by heart rate and is therefore not a true arterial parameter [10].

(iv) A major drawback of the analysis in the PV domain is the fact that time is excluded from the analysis. As we will demonstrate further in this chapter, timing of cardiac and vascular events (contraction and relaxation) is important, especially in the context of ventricular-arterial coupling where timing of reflections will be shown to play a major role on their effective impact on myocardial load.

Assessing Arterial Load with Pressure-Flow Analyses

Whereas assessment of ventricular-arterial coupling in the pressure-volume plane is intuitive and intuitively dissects underlying determinants of stroke volume and LV ejection fraction, ventricular-arterial interactions encompass a wide range of phenomena that are not captured by this approach. Assessment of ventricular-arterial interactions in terms of pulsatile pressure-flow relations provides important incremental information about the physiologic status of the ventricular-arterial system.

At the beginning of each cardiac cycle, the heart generates a forward-traveling energy pulse that results in increased pressure and forward flow in the proximal aorta during early systole [11, 12]. The energy wave generated by the LV (incident wave) is transmitted by conduit vessels and partially reflected at sites of impedance mismatch, such as points of branching or change in wall diameter or material properties along the arterial tree (taking place in a continuous manner due to geometric and mechanical tapering). Multiple small reflections are conducted back to the heart and merge into a "net" reflected wave, composed of the contributions of the scattered backward reflections. Wave dynamics are too complex to fully resolve in vivo and are usually simplified, considering only one forward (generated by the heart) and one backward wave (due to reflections in the periphery). Thus, wave reflections are often analyzed as a single discrete wave, originating from an "effective" reflection site, but this wave is actually the result of scattered reflections, originating from distributed reflection sites (see further). In addition to hemodynamic phenomena related to wave transmission and reflections, the arterial system exerts a buffering function, which depends on its compliance, allowing it to accommodate additional blood volume during systole without excessive increases in pressure and to release that excess volume throughout diastole without excessive drops in pressure [13].

Arterial load can be precisely and comprehensively characterized via analyses of pressure-flow relations (Fig. 4.2). The analysis of arterial input impedance obtained in this manner is considered the gold standard method for the assessment of arterial load [14]. Pressure-flow analyses allow the quantification of "steady" or "resistive" load and various components of pulsatile load [14–17]. The steady component of afterload depends
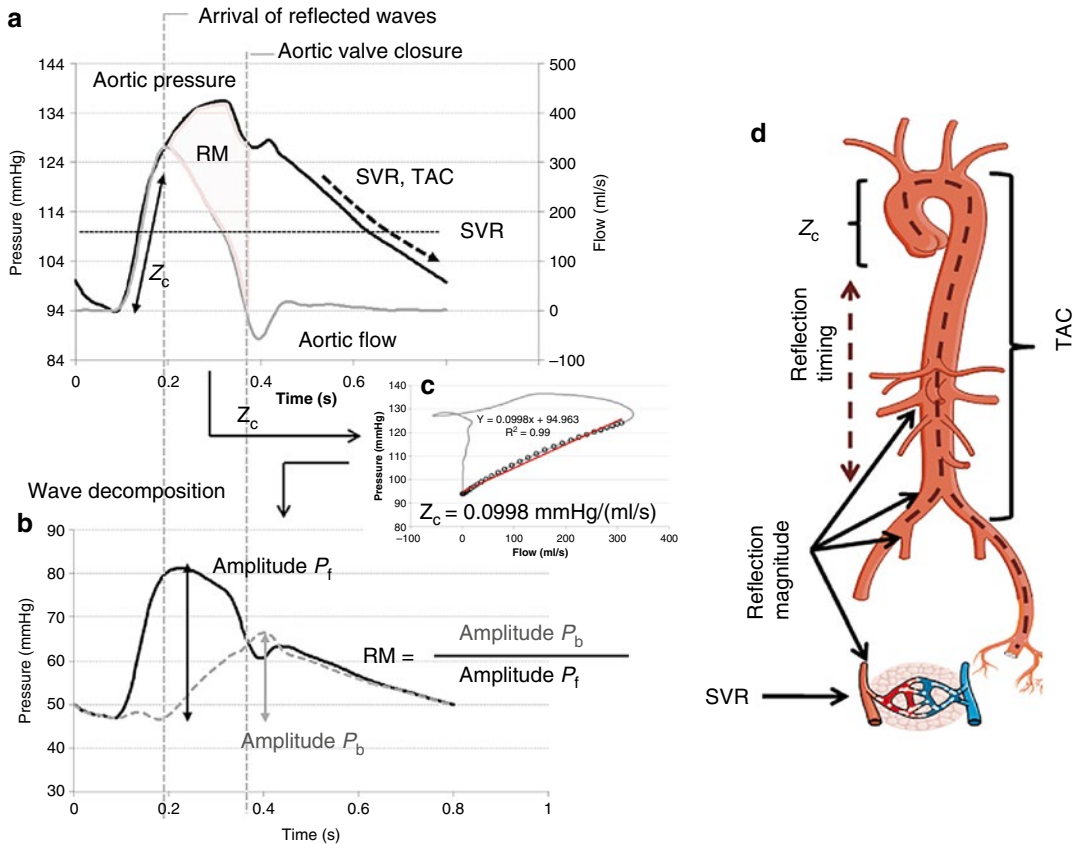
Fig. 4.2 Panel (**a**) Noninvasively acquired carotid pressure and aortic flow waveform, aligned in time. During the early systolic upstroke, in the absence of reflected waves, the pressure and flow waveform are similar in shape, and their ratio determines the characteristic impedance Z_c. When reflected waves kick in, the wave shapes start to deviate, with reflecting generally increasing pressure and decreasing flow. The diastolic pressure decay is determined by the systemic vascular resistance (*SVR*) and total arterial compliance (*TAC*), while SVR also determines the absolute pressure level. Panel (**b**) The result of decomposition of the pressure wave into its forward and backward component. The ratio of their amplitudes is the reflection magnitude (*RM*). Panel (**c**) The computation of RM requires Z_c, which can be estimated from the slope of the linear part of the pressure-flow loop, corresponding to the pressure and flow data prior to the arrival of reflected waves. Panel (**d**) Schematic "anatomical" indication of the components of afterload

largely on the peripheral resistance, which in turn depends on arteriolar caliber, the total number of arterioles that are present "in parallel" and blood viscosity [14, 17]. It can therefore be affected by arteriolar tone, arteriolar remodeling, microvascular rarefaction, and changes in blood viscosity. Pulsatile LV afterload is, in contrast, predominantly influenced by the properties of larger vessels. Although pulsatile LV afterload is fairly complex and cannot be expressed as a single numeric measure, key indices of pulsatile LV afterload can be quantified and summarized using

relatively simple principles and mechanical models of the systemic circulation, using time-resolved proximal aortic pressure and flow.

Time-varying aortic pressure and flow can be assessed invasively or noninvasively (Fig. 4.2, panel a). Noninvasive assessments of central pressure can be achieved using high-fidelity applanation arterial tonometry at the carotid or subclavian [18] artery [14]. Aortic flow can also be measured noninvasively, using pulsed wave Doppler echocardiography [19–21] or phase-contrast magnetic resonance imaging [22]. The most convenient

method to assess aortic inflow is pulsed wave Doppler interrogation of the LV outflow tract, given that systolic LV volume outflow equals proximal aortic volume inflow [21].

LV afterload can be assessed in the frequency domain from the aortic input impedance spectrum (calculated from the harmonic components of central aortic pressure and flow waves) or estimated in the time domain [14, 23–26]. Input impedance is the "summed" mechanical load imposed by all vessels *downstream a particular point* (and which can be fully assessed by measuring time-varying flow and pressure at that particular point) [14, 15, 21, 24]. Therefore, "aortic input impedance" represents the summed mechanical load impeding LV ejection. It should be noted that aortic input impedance is not exclusively determined by aortic properties, but depends on the properties of the entire arterial system.

Key parameters of pulsatile LV load include the characteristic impedance of the proximal aorta (Z_c), the magnitude and timing of wave reflections, and the total compliance of the arterial tree ("total arterial compliance"). The *characteristic* impedance of an artery can be intuitively measured as the slope of the pulsatile pressure-flow relation (where pressure and flow are measured in the same point within the artery) *in the absence of reflected waves*. Aortic Z_c can thus be computed in the time domain using the slope of the pressure change over flow change in early systole, before the arrival of wave reflections to the proximal aorta (Fig. 4.2, panel c). Z_c is a "local" arterial property (note the difference with *input* impedance); consequently, Z_c measured using proximal aortic pressure and flow represents proximal aortic Z_c. Physically, Z_c reflects the balance between inertial and capacitive effects in the aorta upon cardiac ejection. In a rigid and/or narrowed aorta, blood cannot be stored locally, and blood needs to be accelerated instantaneously throughout the complete aorta, leading to high characteristic impedance. In a wide and/or distensible aorta, blood is stored locally due to the windkessel effect, and acceleration of blood takes place over much shorter lengths and is dampened in time, reducing inertial effects and characteristic impedance.

Wave reflections are usually assessed via *wave separation analysis*, based on the principle that reflected waves, by virtue of adding to pressure and subtracting from forward flow, distort the linear relationship between pulsatile pressure and flow that is seen in early systole (as a result of the forward wave generated by ventricular contraction), when such relationship is governed purely by ascending aortic Z_c (Fig. 4.2, panel b). The ratio of the amplitude of the backward (reflected) and forward wave yields the reflection magnitude (RM).

Making abstraction of wave travel and reflection, one can also consider the arterial tree as a condensed windkessel-like system, of which the "total arterial compliance" (TAC) can be computed using windkessel models of the arterial tree. Frank proposed the original windkessel model as a resistance and compliance (*C*) pair (2-element windkessel), representing small vessel resistance and large artery compliance. The 3-element windkessel model additionally accounts for aortic characteristic impedance (Z_c) in order to better capture the behavior of the arterial tree for the higher frequency range and to isolate the "slow" effects of compliance in diastole from the "rapid" effects associated with wave dynamics during cardiac ejection [26]. This model, originally proposed by Westerhof et al., can be considered the standard windkessel model for the systemic circulation, although refinements have been proposed by Westerhof [27], as well as several other investigators (see Ref. [13] for review).

Determinants of Pulsatile Arterial Load

The geometric and mechanical properties of the various arterial segments have complex effects on ventricular afterload; through their effects on the early aortic systolic pressure rise, the total compliance of the arterial system and the velocity at which the pulse waves travel forward in the arteries and reflected waves originate and travel backward toward the heart [25, 28]. In early systole, a high proximal aortic characteristic impedance (Z_c) due to a stiff wall, a small aortic diameter, or both increases the amount of pulsatile pressure for

any given pulsatile flow [11–14]. The time of arrival of the reflected wave to the proximal aorta depends on the location of reflection sites and on the pulse wave velocity (PWV) of conduit vessels, particularly the aorta, which transmits both the forward and backward traveling waves [12, 14]. Aortic PWV is directly related to the stiffness of the aortic wall (square root of elastic modulus) and inversely proportional to the square root of aortic diameter [12, 14, 29]. Stiffer aortas thus conduct the forward and backward traveling waves at greater velocity and therefore promote an earlier arrival of the reflected wave for any given distance to reflection sites. The distance to the reflection sites is strongly dependent on body height. In the presence of normal LV systolic function, typical effects of the reflected wave on the aortic pressure waveform include a mid-to-late systolic shoulder which determines an increase in peak (systolic) aortic pressure (and pulse pressure) and the area under the pressure curve during systole [14]. When LV systolic function is depressed, however, the reflected wave may induce a reduction on late systolic flow with less prominent effects of pressure augmentation.

The total arterial compliance depends on the summed compliance of the various arterial segments. The compliance of individual vessels is (linearly) proportional to vessel volume (or radius [3]) and, for any given "relative" vessel geometry (wall volume/lumen volume ratio), (linearly and) inversely proportional to wall stiffness (Young's elastic modulus). The interaction between the stiffness and geometry of large and muscular arteries also impacts the magnitude and location of reflection sites. Reflected waves that arrive during LV ejection increase the mid-to-late systolic workload of the LV. Figure 4.2, panel d, illustrates the different components of LV afterload.

A Time-Domain Approach to Ventricular-Arterial Coupling: Time-Varying Myocardial Stress

Pressure-flow analyses thoroughly characterize the interactions between the LV (treated as a hydraulic pump) and the arterial system and provide important indices of arterial load and

cardiac function. Various indices of LV afterload are useful because they are meant to be purely reflective of arterial properties [14]. However, arterial load should always be interpreted by considering interactions between arteries and the LV as a pump [14, 30] and also between myocardial elements and instantaneous LV geometry and the time-varying load imposed by the systemic circulation. The generation of pressurized blood flow by the LV can be conceptually represented by a 2-step energy transfer process: first from the contractile elements of the myocardium into the LV chamber and second from the LV chamber to the systemic circulation. However, this process is bidirectional, such that the systemic circulation can also impact the myocardial contractile elements. Wall stress represents the time-varying mechanical load experienced by the contractile elements in the myocardium (myocardial afterload) and is related to the amount of force and work the muscle does during a contraction.

Whereas wall stress has been recognized as a key index of myocardial load, until recently, it was assessed only in end-systole, in analogy to the LV elastance, which reaches a peak in end-systole. However, derivations of Laplace's law indicate that the progressive geometric changes that accompany the ejection of blood from the LV into the arteries will be associated with important changes in wall stress, favoring a reduction of wall stress in late systole. This motivated the development of methods to assess time-resolved myocardial wall stress [31, 32]. There are several methods to estimate wall stress using LV geometric and LV pressure measurements. A particularly useful formula, applicable to axisymmetric ventricles for computation of average LV myocardial fiber stress, was developed by Arts et al. [31] and may be used for calculating time-resolved ejection-phase fiber stress using a central pressure waveform (given that in the absence of aortic stenosis, central arterial pressure is very similar to ventricular pressure) and time-resolved LV geometric information (derived from 2D echocardiography, 3D echocardiography, or magnetic resonance imaging) [25, 31–34]. This method, illustrated in Fig. 4.3, does not neglect radially directed forces or forces generated within the wall that oppose fiber shortening, which vary significantly with cavity and wall
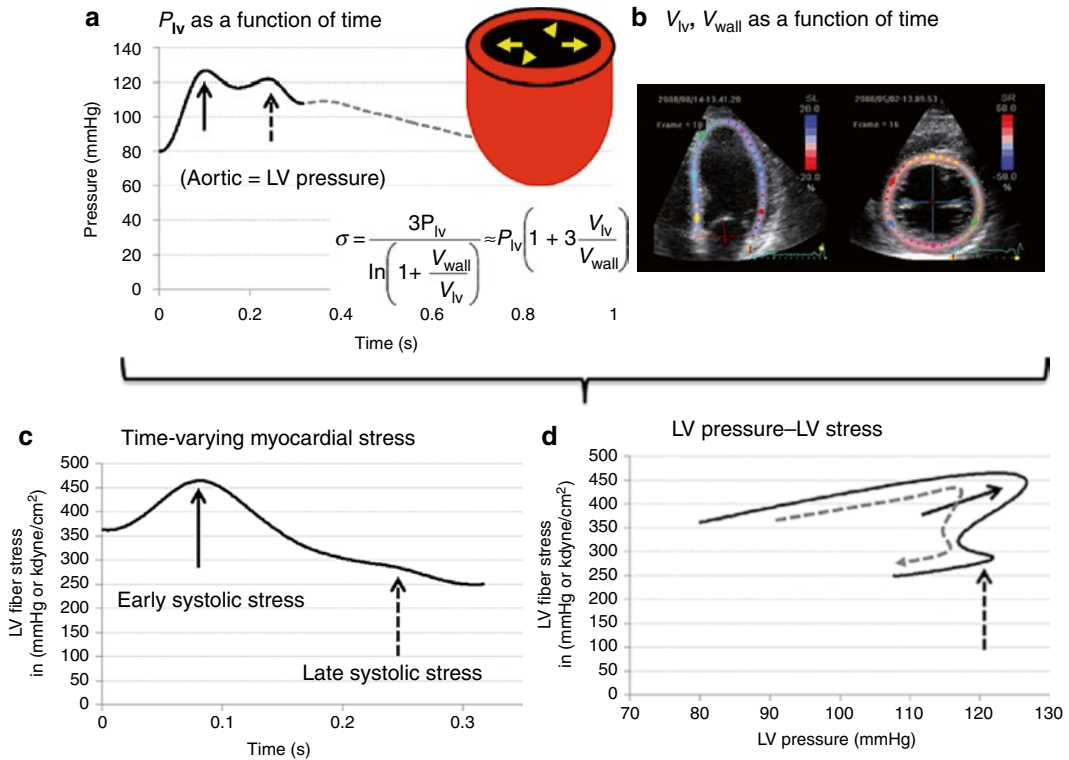
a P_{lv} as a function of time

(Aortic = LV pressure)

$$\sigma = \frac{3P_{lv}}{\ln\left(1 + \dfrac{V_{wall}}{V_{lv}}\right)} \approx P_{lv}\left(1 + 3\frac{V_{lv}}{V_{wall}}\right)$$

b V_{lv}, V_{wall} as a function of time

c Time-varying myocardial stress

Early systolic stress

Late systolic stress

d LV pressure–LV stress

Fig. 4.3 Panel (**a**) Assuming identical aortic and left ventricular pressures during systole, LV pressure can be obtained from a noninvasively measured pressure waveform. Panel (**b**) Combined with time-varying geometric information, which can be measured with ultrasound or MRI, time-varying myocardial stress can be calculated using the formula provided by Arts et al. [31]. Panel (**c**) Time-varying myocardial stress, peaking in early systole. The second pressure peak in late systole does not lead to a high end-systolic stress. Panel (**d**) LV fiber stress plotted as a function of LV pressure, clearly demonstrating the "shift" in stress throughout ejection

thickness and can interfere with direct comparisons of myocardial fiber stress at different times during ejection. The formula is based on LV cavity volume (V_{lv}), LV wall volume (V_{wall}), and pressure:

$$\text{Fiber}\,\sigma = \frac{P}{\frac{1}{3}\ln\left(1 + \dfrac{V_{wall}}{V_{lv}}\right)}$$

It is important to recognize the advantages of assessing time-resolved ejection-phase LV wall stress as opposed to end-systolic wall stress. Throughout systole, myocardial fiber activation results in the development of tension (stress) and shortening of myocardial segments, which results in progressive ejection of blood from the LV cavity and wall thickening. During *early* ejection, active development of fiber crossbridges occurs in the electrically activated myocardium, and peak myocardial wall stress occurs [32], at a time when systolic pressure coexists with quasi-diastolic geometry (relatively thin wall and relatively large cavity) (Fig. 4.3, panel c). Myocardial fiber shortening and ejection of blood determine a progressive change in LV geometry, which causes a drop in myocardial stress (despite rising pressure) during mid-to-late systole. This can be quantified as a clear "shift" in the pressure-stress relation (Fig. 4.3, panel d) and appears to be favorable for the myocardium to handle the additional load imposed by systolic wave reflections, which are "universal" in adults. This shift, however, may be insufficient and/or compromised in the setting of wave reflections of early onset or large magnitude [34–36] and in the presence of a depressed LV ejection fraction [32, 35]. A time-resolved wall stress curve also allows for characterization of the *myocardial* loading sequence,

which can be expressed as a ratio of the stress-time integral in late vs. early systole. We note that stress as calculated here encompasses both the active stress generated by active mechanisms in the muscle fibers as well as passively induced stresses in both the cellular and extracellular matrix components of the ventricle.

Determinants of Time-Varying Myocardial Stress: Impact of Wave Reflections

In addition to the well-known role of chronic ventricular geometric changes as determinants of wall stress, as expected from physiologic principles, various arterial properties affect time-varying myocardial wall stress for any given end-diastolic LV geometry [34]. Systemic vascular resistance is a very important determinant of wall stress throughout systole. Z_c selectively affects early systolic and peak systolic wall stress, whereas wave reflections and total arterial compliance impact myocardial stress in mid and late systole and significantly influence the area under the stress curve generated for any given flow output [34]. Interestingly, women seem to demonstrate greater peak and end-systolic wall stress as well as a higher ejection-phase stress-time integral, even after adjustment for arterial properties, which might relate to the differential susceptibility of women to heart failure [34].

Importance of Late Systolic Load: Animal, Epidemiologic, and Clinical Studies of Wave Reflections, Myocardial Function, and Heart Failure Risk

Late Systolic Loading from Wave Reflections Leads to LV Hypertrophy

For any given level of systolic (peak) blood pressure, prominent late systolic loading has been unequivocally demonstrated to exert deleterious effects on LV structure and function in animal models and has been associated with LV hypertrophy in humans [14, 37, 38]. Kobayashi et al. [37] used a Wistar rat model and performed constriction of either the ascending aorta or suprarenal abdominal aorta. Analysis of aortic input impedance demonstrated that constriction of the ascending aorta increased LV load in early systole, whereas constriction of the descending aorta caused prominent late systolic loading from a reflected wave that originated at the distal aortic constriction site, arriving at the heart in late systole [37]. LV pressure profiles induced by proximal aortic constriction demonstrated an early systolic peak, whereas descending aortic constriction induced late systolic peaks. Despite an identical peak LV pressure in rats that underwent ascending vs. descending aortic constriction, rats that underwent descending aortic banding (and were thus exposed to greater late systolic load) demonstrated much greater LV hypertrophy than those undergoing ascending aortic banding (which were exposed to increased early systolic load). Rats that underwent descending aortic banding also demonstrated a greater amount of myocardial fibrosis [37].

These animal causal findings are strongly supported by observational human data. Hashimoto et al. [39] assessed changes in wave reflection magnitude occurring during antihypertensive therapy and observed that the reduction in wave reflections predicted regression of LV mass independently of blood pressure reduction. The association between reflected wave magnitude reduction and LV mass (i.e., hypertrophy) reduction was also independent of age, sex, and use of renin-angiotensin system inhibitors ($\beta=0.41$, $P=0.001$). The correlation was particularly strong in patients with LV hypertrophy at baseline ($R=0.61$; $P<0.001$). Of note, despite the fact that standard antihypertensive therapies reduce wave reflections in some patients, the change is highly unpredictable, with reflection magnitude actually increasing in some subjects in Hashimoto's study, despite blood pressure reduction.

Late Systolic Load Promotes Diastolic Dysfunction

Gillebert et al. [38] used a canine model to study the effect of the *timing* of systolic load on LV relaxation by inflating balloons in the ascending
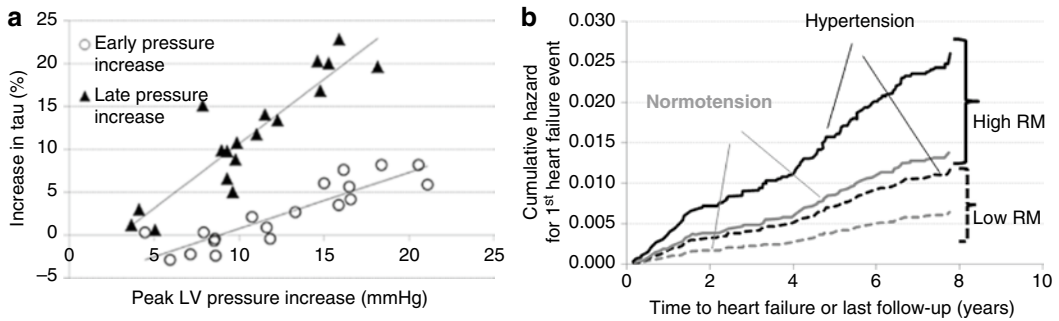
Fig. 4.4 Panel (**a**) Impact of timing of afterload on the time constant of LV relaxation (tau). Late pressure increase has a much more pronounced effect on LV relaxation than an increase in early systole (Modified from Gillebert et al. [38]). Panel (**b**) Impact of reflection magnitude (*RM*) on hazard of heart failure (Modified from Chirinos et al. [47])

aorta during either early vs. late systole. Their study demonstrated that for a given increase in peak (systolic) LV pressure, late systolic inflation (triangles in Fig. 4.4a) prolonged *tau* (i.e., impaired LV relaxation assessed with the gold standard measure) much more than early systolic inflation (circles in Fig. 4.4a), demonstrating a cause-effect relationship between late systolic load and diastolic dysfunction [38].

In support of these causal findings, wave reflections have been independently linked to diastolic dysfunction in human clinical cohorts [40, 41]. Borlaug et al. demonstrated that late systolic load (assessed with the late systolic pressure-time integral) was associated with lower early diastolic mitral annular tissue velocities (a marker of diastolic function) among 48 hypertensive and normotensive subjects [42]. Ikonomidis showed that augmentation index was independently associated with diastolic dysfunction among 143 hypertensive patients [43]. Weber et al. [41] studied 336 patients undergoing coronary angiography and showed that augmentation index and augmented pressure (which are influenced by wave reflections) were associated with lower peak mitral annular systolic velocity, early diastolic velocity, and higher LV filling pressures.

Recently, we used time-resolved stress curves to separate early and late systolic wall stress (i.e., early vs. late myocardial systolic load), which can be quantified as the area under the time-resolved stress curve (stress-time integral, STI) in the first and second halves of ejection, respectively, among

[33, 34] middle-aged adults enrolled in the population-based Asklepios study in Belgium [32, 34, 44–46]. We assessed the relationship between the myocardial loading sequence (early vs. late wall stress) and diastolic function [33]. After adjustment for multiple confounders, late systolic load was independently associated with lower mitral annular relaxation velocities, in sharp contrast to early systolic load which was associated with higher mitral annular relaxation velocities, in a multivariate model, implicating the loading sequence as an independent correlate of myocardial relaxation in humans. This model explained 46 % of the variability in mitral annular diastolic (relaxation) velocity.

The Magnitude of Wave Reflections Strongly Predicts New-Onset Heart Failure in the General Population

Based on the data presented above, we hypothesized that wave reflections independently predict the risk of new-onset heart failure (HF) in the general population. To test this hypothesis, we derived aortic pressure waveforms using a transfer function applied to the radial waveform recorded at baseline with arterial tonometry from 5,934 participants in the Multiethnic Study of Atherosclerosis (MESA), who were free of clinically apparent cardiovascular disease. The central pressure waveform was used to assess reflection magnitude [35, 47]. During 7.61 years

of follow-up (and after adjustment for systolic and diastolic blood pressure, age, gender, body mass index, diabetes, ethnicity, antihypertensive medication use, total and HDL cholesterol, current smoking, heart rate, and glomerular filtration rate), reflection magnitude strongly predicted HF (hazard ratio per 10 % – increase = 2.69; 95 % CI = 1.79–4.04; $P < 0.0001$) and was a stronger predictor than blood pressure and all other modifiable risk factors listed above.

When we stratified the population based on the presence or absence of hypertension and the presence or absence of high reflection magnitude (Fig. 4.4b), we found that, compared to non-hypertensive subjects with low reflection magnitude (lowest risk category), hazard ratios for hypertensive subjects with low reflection magnitude, non-hypertensive subjects with high reflection magnitude, and hypertensive subjects with high reflection magnitude were 1.81 (95 % CI = 0.85–3.86), 2.16 (95 % CI = 1.04–4.43), and 3.98 (95 % CI = 1.96–8.05), respectively. We also assessed the incremental information provided when various predictors were added to a model containing all other predictors of heart failure, in terms of discrimination (integrated discrimination improvement) and reclassification (net reclassification improvement). Reflection magnitude was associated with the largest Wald statistic of all predictors (including age), the greatest reduction in Akaike's information and Bayesian information criteria (indicating improvement in model fit) and the greatest increases in integrated discrimination improvement (with a 48 % increase in discrimination slope achieved when reflection magnitude was added to a base model containing all other predictors of HF and multiple confounders). With the exception of age, a non-modifiable risk factor, reflection magnitude was associated with the greatest net reclassification improvement for prediction of HF. Therefore, reflection magnitude was a strong predictor of incident HF after adjustment for other known predictors. These findings from a large community-based sample with careful follow-up and event adjudication implicate arterial wave reflections as a novel strong risk factor for HF, thus strongly supporting animal and human

mechanistic findings from previous studies and demonstrating the relevance of wave reflections in humans. Based on the strength and biologic plausibility of this association, a high reflection magnitude has been proposed to represent a novel form of stage B HF [35].

The Reflected Wave in Established HF

Early invasive studies demonstrated enhanced wave reflections in patients with systolic HF compared to normal control subjects, with an impaired reduction of wave reflections during exercise [48, 49]. More recently, wave reflections assessed noninvasively have been reported to be increased in patients with established systolic HF and heart failure with preserved ejection fraction (HFpEF). Curtis et al. reported increased wave reflections (assessed via wave intensity analysis) among 67 patients with systolic HF [50]. Recently, Weber et al. demonstrated that a high reflected wave is a good index to identify patients with HFpEF among individuals presenting with dyspnea [51]. Importantly, Sung et al. reported that, among 120 patients hospitalized due to decompensated HF (~56 % with systolic heart failure and 44 % with HFpEF), reflected wave amplitude, but not carotid-femoral pulse wave velocity, was an independent predictor of rehospitalization for HF, all-cause death, nonfatal myocardial infarction and stroke, after adjustment for age, estimated glomerular filtration rate, hemoglobin, and NT-proBNP levels [52].

Where Do Wave Reflections Originate?

Wave reflections arise at any point of impedance mismatch, impedance being here the local characteristic impedance at a given point in the arterial tree. As previously mentioned, it is virtually impossible to unequivocally pinpoint the source(s) of wave reflections. Inspired by the nature of the input impedance and the concept of the "effective length" of the arterial tree [53], researchers attempted to identify "the" dominant

reflection site(s) of the arterial tree. The aortoiliac bifurcation [54–57], diaphragm level (and branches toward renal arteries and gastrointestinal organs) [55, 58], and head and upper extremities [57] have been proposed as candidate discrete reflection sites. Nevertheless, the observed reflection patterns do not fully match these of a discrete number of reflection sites [54], suggesting the presence of diffuse reflections, originating all over the arterial tree [59, 60]. These diffuse reflections are due to the branching pattern of the aorta, the effect of geometric and mechanical tapering (leading to a continuous change in local characteristic impedance [61]) but most certainly also due to the resistance vessels, where impedance rapidly increases over very short distances (also leading to an abrupt drop in mean arterial pressure). The presence of reflections close to the heart also seems to obscure reflections arising from further down in the arterial tree, creating sort of a "horizon effect" [62].

It is clear that wave reflections are complex, and this complexity should be considered and taken into account when interpreting hemodynamic data. The paradigm of the arterial tree as a single uniform tube with a discrete reflection occurring at a fixed length is certainly too simple an approach, giving rise to controversies [63–65]. What is also clear is that the sources of wave reflections are not to be sought only distally in the arterial tree, but also closer to the heart. It is well known that wave reflection can be modulated pharmacologically, where the administration of nitroglycerin (NTG) clearly leads to a reduction in wave reflections [66]. NTG is thought to act on peripheral muscular vessels [67]. However, it is possible that NTG also affects vessels closer to the heart. Abdominal organs are relatively close to the heart, and their perfusion is regulated by vasoactive mechanisms. As such, the impact of NTG on wave reflections may be related to vasodilation of splanchnic vessels, as also suggested by Karamanoglu et al. [58]. It is not clear whether there is also an effect on the arterial tone of larger vessels such as the abdominal aorta. We refer to Chap. 40 of this book for an in-depth discussion on the effect of organic nitrates.

Conclusions and Future Directions

Advances in the noninvasive assessment of pressure-flow relations and noninvasive cardiac imaging now allow for a comprehensive noninvasive assessment of ventricular-arterial interactions/coupling and should be more widely applied in clinical research. In particular, whereas analyses of ventricular-arterial coupling in the pressure-volume plane provide a simple, intuitive, and useful framework, it provides limited information, and other comprehensive noninvasive hemodynamic assessments should be more widely applied in human studies. Given the importance of LV afterload and its impact on the heart, afterload should be carefully considered or ruled out as a potential mediator or confounder in a wide variety of observed relationships or therapeutic and adverse effects of interventions related to LV remodeling, LV function, or vasoactive interventions.

Modeling approaches for pressure, flow, and geometric data are likely to continue to evolve, allowing for a more accurate assessment of hemodynamic patterns and their effects on cardiac load and function. This should lead to a better and generally accepted quantification and understanding of wave reflections, their origin, and their role in the pathophysiology of cardiovascular diseases. Carefully designed randomized clinical trials in the next decade may allow these insights to be used in the management of patients at risk for, or those with established, cardiovascular disease.

References

1. Sunagawa K, Maughan WL, Burkhoff D, Sagawa K. Left ventricular interaction with arterial load studied in isolated canine ventricle. Am J Physiol. 1983;245:H773–80.
2. Suga H, Sagawa K. Instantaneous pressure-volume relationships and their ratio in the excised, supported canine left ventricle. Circ Res. 1974;35:117–26.
3. Kelly RP, Ting CT, Yang TM, Liu CP, Maughan WL, Chang MS, Kass DA. Effective arterial elastance as index of arterial vascular load in humans. Circulation. 1992;86:513–21.
4. Burkhoff D, Sagawa K. Ventricular efficiency predicted by an analytical model. Am J Physiol. 1986;250:R1021–7.

5. Suga H, Hayashi T, Shirahata M. Ventricular systolic pressure-volume area as predictor of cardiac oxygen consumption. Am J Physiol. 1981;240:H39–44.

6. Chen CH, Nakayama M, Nevo E, Fetics BJ, Maughan WL, Kass DA. Coupled systolic-ventricular and vascular stiffening with age: implications for pressure regulation and cardiac reserve in the elderly. J Am Coll Cardiol. 1998;32:1221–7.

7. Ishihara H, Yokota M, Sobue T, Saito H. Relation between ventriculoarterial coupling and myocardial energetics in patients with idiopathic dilated cardiomyopathy. J Am Coll Cardiol. 1994;23:406–16.

8. Sasayama S, Asanoi H. Coupling between the heart and arterial system in heart failure. Am J Med. 1991;90:14S–8.

9. van der Velde ET, Burkhoff D, Steendijk P, Karsdon J, Sagawa K, Baan J. Nonlinearity and load sensitivity of end-systolic pressure-volume relation of canine left ventricle in vivo. Circulation. 1991;83:315–27.

10. Segers P, Stergiopulos N, Westerhof N. Relation of effective arterial elastance to arterial system properties. Am J Physiol Heart Circ Physiol. 2002;282:H1041–6.

11. Segers P, Stergiopulos N, Westerhof N. Quantification of the contribution of cardiac and arterial remodeling to hypertension. Hypertension. 2000;36:760–5.

12. Mitchell GF. Arterial stiffness and wave reflection in hypertension: pathophysiologic and therapeutic implications. Curr Hypertens Rep. 2004;6:436–41.

13. Westerhof N, Lankhaar JW, Westerhof BE. The arterial windkessel. Med Biol Eng Comput. 2009;47:131–41.

14. Nichols WW, O'Rourke MF, Vlachopolous C. Mcdonald's blood flow in arteries. Theoretical, experimental and clinical principles. London: Hodder Arnold; 2011.

15. Segers P, Verdonck P. Principles of vascular physiology. In: Lanzer P, Topol E, editors. Panvascular medicine: integrated clinical management. Berlin/Heidelberg: Springer; 2002.

16. O'Rourke MF, Safar ME. Relationship between aortic stiffening and microvascular disease in brain and kidney: cause and logic of therapy. Hypertension. 2005;46:200–4.

17. Ooi H, Chung W, Biolo A. Arterial stiffness and vascular load in heart failure. Congest Heart Fail. 2008;14:31–6.

18. Aakhus S, Soerlie C, Faanes A, Hauger SO, Bjoernstad K, Hatle L, Angelsen BA. Noninvasive computerized assessment of left ventricular performance and systemic hemodynamics by study of aortic root pressure and flow estimates in healthy men, and men with acute and healed myocardial infarction. Am J Cardiol. 1993;72:260–7.

19. Mitchell GF, Lacourciere Y, Arnold JM, Dunlap ME, Conlin PR, Izzo Jr JL. Changes in aortic stiffness and augmentation index after acute converting enzyme or vasopeptidase inhibition. Hypertension. 2005;46:1111–7.

20. Mitchell GF, Lacourciere Y, Ouellet JP, Izzo Jr JL, Neutel J, Kerwin LJ, Block AJ, Pfeffer MA. Determinants of elevated pulse pressure in middle-aged

and older subjects with uncomplicated systolic hypertension: the role of proximal aortic diameter and the aortic pressure-flow relationship. Circulation. 2003;108:1592–8.

21. Segers P, Rietzschel ER, De Buyzere ML, Vermeersch SJ, De Bacquer D, Van Bortel LM, De Backer G, Gillebert TC, Verdonck PR. Noninvasive (input) impedance, pulse wave velocity, and wave reflection in healthy middle-aged men and women. Hypertension. 2007;49:1248–55.

22. Gatehouse PD, Keegan J, Crowe LA, Masood S, Mohiaddin RH, Kreitner KF, Firmin DN. Applications of phase-contrast flow and velocity imaging in cardiovascular mri. Eur Radiol. 2005;15:2172–84.

23. Kass DA. Ventricular arterial stiffening: integrating the pathophysiology. Hypertension. 2005;46:185–93.

24. Mitchell GF. Clinical achievements of impedance analysis. Med Biol Eng Comput. 2009;47:153–63.

25. Chirinos JA, Segers P. Noninvasive evaluation of left ventricular afterload: part 2: arterial pressure-flow and pressure-volume relations in humans. Hypertension. 2010;56:563–70.

26. Segers P, Rietzschel ER, De Buyzere ML, Stergiopulos N, Westerhof N, Van Bortel LM, Gillebert T, Verdonck PR. Three- and four-element windkessel models: assessment of their fitting performance in a large cohort of healthy middle-aged individuals. Proc Inst Mech Eng H. 2008;222:417–28.

27. Stergiopulos N, Westerhof BE, Westerhof N. Total arterial inertance as the fourth element of the windkessel model. Am J Physiol. 1999;276:H81–8.

28. Chirinos JA, Segers P. Noninvasive evaluation of left ventricular afterload: part 1: pressure and flow measurements and basic principles of wave conduction and reflection. Hypertension. 2010;56:555–62.

29. Chirinos JA. Arterial stiffness: basic concepts and measurement techniques. J Cardiovasc Transl Res. 2012;5:243–55.

30. Kawaguchi M, Hay I, Fetics B, Kass DA. Combined ventricular systolic and arterial stiffening in patients with heart failure and preserved ejection fraction: implications for systolic and diastolic reserve limitations. Circulation. 2003;107:714–20.

31. Arts T, Bovendeerd PH, Prinzen FW, Reneman RS. Relation between left ventricular cavity pressure and volume and systolic fiber stress and strain in the wall. Biophys J. 1991;59:93–102.

32. Chirinos JA, Segers P, Gupta AK, Swillens A, Rietzschel ER, De Buyzere ML, Kirkpatrick JN, Gillebert TC, Wang Y, Keane MG, Townsend R, Ferrari VA, Wiegers SE, St John Sutton M. Time-varying myocardial stress and systolic pressure-stress relationship: role in myocardial-arterial coupling in hypertension. Circulation. 2009;119:2798–807.

33. Chirinos JA, Segers P, Rietzschel ER, De Buyzere ML, Raja MW, Claessens T, De Bacquer D, St John Sutton M, Gillebert T, Asklepios Investigators. Early and late systolic wall stress differentially relate to myocardial contraction and relaxation in middle-aged adults. The asklepios study. Hypertension. 2013;61:296–303.

34. Chirinos JA, Segers P, Gillebert TC, Gupta AK, De Buyzere ML, De Bacquer D, St John-Sutton M, Rietzschel ER. Arterial properties as determinants of time-varying myocardial stress in humans. Hypertension. 2012;60:64–70.

35. Shah SJ, Wasserstrom JA. Increased arterial wave reflection magnitude: a novel form of stage b heart failure? J Am Coll Cardiol. 2012;60:2178–81.

36. Chowienczyk P, Shah A. Myocardial wall stress: from hypertension to heart tension. Hypertension. 2012;60:10–1.

37. Kobayashi S, Yano M, Kohno M, Obayashi M, Hisamatsu Y, Ryoke T, Ohkusa T, Yamakawa K, Matsuzaki M. Influence of aortic impedance on the development of pressure-overload left ventricular hypertrophy in rats. Circulation. 1996;94:3362–8.

38. Gillebert TC, Lew WY. Influence of systolic pressure profile on rate of left ventricular pressure fall. Am J Physiol. 1991;261:H805–13.

39. Hashimoto J, Westerhof BE, Westerhof N, Imai Y, O'Rourke MF. Different role of wave reflection magnitude and timing on left ventricular mass reduction during antihypertensive treatment. J Hypertens. 2008;26:1017–24.

40. Fukuta H, Ohte N, Wakami K, Asada K, Goto T, Mukai S, Tani T, Kimura G. Impact of arterial load on left ventricular diastolic function in patients undergoing cardiac catheterization for coronary artery disease. Circ J. 2010;74:1900–5.

41. Weber T, O'Rourke MF, Ammer M, Kvas E, Punzengruber C, Eber B. Arterial stiffness and arterial wave reflections are associated with systolic and diastolic function in patients with normal ejection fraction. Am J Hypertens. 2008;21:1194–202.

42. Borlaug BA, Melenovsky V, Redfield MM, Kessler K, Chang HJ, Abraham TP, Kass DA. Impact of arterial load and loading sequence on left ventricular tissue velocities in humans. J Am Coll Cardiol. 2007;50:1570–7.

43. Ikonomidis I, Tzortzis S, Papaioannou T, Protogerou A, Stamatelopoulos K, Papamichael C, Zakopoulos N, Lekakis J. Incremental value of arterial wave reflections in the determination of left ventricular diastolic dysfunction in untreated patients with essential hypertension. J Hum Hypertens. 2008;22:687–98.

44. Chirinos JA, Rietzschel ER, De Buyzere ML, De Bacquer D, Gillebert TC, Gupta AK, Segers P. Arterial load and ventricular-arterial coupling: physiologic relations with body size and effect of obesity. Hypertension. 2009;54:558–66.

45. Chirinos JA, Segers P, De Buyzere ML, Kronmal RA, Raja MW, De Bacquer D, Claessens T, Gillebert TC, St John-Sutton M, Rietzschel ER. Left ventricular mass: allometric scaling, normative values, effect of obesity, and prognostic performance. Hypertension. 2010;56:91–8.

46. Chirinos JA, Segers P, Rietzschel ER, De Buyzere ML, Raja MW, Claessens T, De Bacquer D, St John Sutton M, Gillebert TC. Early and late systolic wall stress differentially relate to myocardial contraction and relaxation in middle-aged adults: the asklepios study. Hypertension. 2013;61:296–303.

47. Chirinos JA, Kips JG, Jacobs Jr DR, Brumback L, Duprez DA, Kronmal R, Bluemke DA, Townsend RR, Vermeersch S, Segers P. Arterial wave reflections and incident cardiovascular events and heart failure: Mesa (multiethnic study of atherosclerosis). J Am Coll Cardiol. 2012;60:2170–7.

48. Laskey WK, Kussmaul WG. Arterial wave reflection in heart failure. Circulation. 1987;75:711–22.

49. Pepine CJ, Nichols WW, Conti CR. Aortic input impedance in heart failure. Circulation. 1978;58:460–5.

50. Curtis SL, Zambanini A, Mayet J, Mc GTSA, Foale R, Parker KH, Hughes AD. Reduced systolic wave generation and increased peripheral wave reflection in chronic heart failure. Am J Physiol Heart Circ Physiol. 2007;293:H557–62.

51. Weber T, Wassertheurer S, O'Rourke MF, Haiden A, Zweiker R, Rammer M, Hametner B, Eber B. Pulsatile hemodynamics in patients with exertional dyspnea: potentially of value in the diagnostic evaluation of suspected heart failure with preserved ejection fraction. J Am Coll Cardiol. 2013;61:1874–83.

52. Sung SH, Yu WC, Cheng HM, Lee CW, Lin MM, Chuang SY, Chen CH. Excessive wave reflections on admission predict post-discharge events in patients hospitalized due to acute heart failure. Eur J Heart Fail. 2012;14:1348–55.

53. Campbell KB, Lee LC, Frasch HF, Noordergraaf A. Pulse reflection sites and effective length of the arterial system. Am J Physiol. 1989;256:H1684–9.

54. Pythoud F, Stergiopulos N, Westerhof N, Meister JJ. Method for determining distribution of reflection sites in the arterial system. Am J Physiol. 1996;271:H1807–13.

55. Latham RD, Westerhof N, Sipkema P, Rubal BJ, Reuderink P, Murgo JP. Regional wave travel and reflections along the human aorta: a study with six simultaneous micromanometric pressures. Circulation. 1985;72:1257–69.

56. Murgo JP, Westerhof N, Giolma JP, Altobelli SA. Aortic input impedance in normal man: relationship to pressure wave forms. Circulation. 1980;62:105–16.

57. O'Rourke MF. Pressure and flow waves in systemic arteries and the anatomical design of the arterial system. J Appl Physiol. 1967;23:139–49.

58. Karamanoglu M, Gallagher DE, Avolio AP, O'Rourke MF. Functional origin of reflected pressure waves in a multibranched model of the human arterial system. Am J Physiol. 1994;267:H1681–8.

59. O'Rourke MF, Taylor MG. Input impedance of the systemic circulation. Circ Res. 1967;20:365–80.

60. Taylor MG. The input impedance of an assembly of randomly branching elastic tubes. Biophys J. 1966;6:29–51.

61. Segers P, Verdonck P. Role of tapering in aortic wave reflection: hydraulic and mathematical model study. J Biomech. 2000;33:299–306.

62. Davies JE, Alastruey J, Francis DP, Hadjiloizou N, Whinnett ZI, Manisty CH, Aguado-Sierra J, Willson K, Foale RA, Malik IS, Hughes AD, Parker KH, Mayet J. Attenuation of wave reflection by wave entrapment creates a "horizon effect" in the human aorta. Hypertension. 2012;60:778–85.

63. Segers P, Mynard J, Taelman L, Vermeersch S, Swillens A. Wave reflection: myth or reality? Artery Res. 2012;6:7–11.

64. Segers P, Kips J, Trachet B, Swillens A, Vermeersch S, Mahieu D, Rietzschel ER, De Buyzere M, Van Bortel L. Limitations and pitfalls of non-invasive measurement of arterial pressure wave reflections and pulse wave velocity. Artery Res. 2009;3:79–88.

65. Westerhof BE, Westerhof N. Magnitude and return time of the reflected wave: the effects of large artery stiffness and aortic geometry. J Hypertens. 2012;30:932–9.

66. Kelly RP, Gibbs HH, O'Rourke MF, Daley JE, Mang K, Morgan JJ, Avolio AP. Nitroglycerin has more favourable effects on left ventricular afterload than apparent from measurement of pressure in a peripheral artery. Eur Heart J. 1990;11: 138–44.

67. Pauca AL, Kon ND, O'Rourke MF. Benefit of glyceryl trinitrate on arterial stiffness is directly due to effects on peripheral arteries. Heart. 2005;91: 1428–32.